

Influence of graphene additives on dynamic strength and failure of alumina under shock loading

© G.G. Savenkov,^{1,2,3} A.Yu. Konstantinov,⁴ A.V. Kuznetsov,³ M.A. Pakhomov,⁵ V.V. Stolyarov⁵

¹ St. Petersburg State Technological Institute (Technical University), St. Petersburg, Russia

² Ioffe Institute, St. Petersburg, Russia

³ JSC „Armalit“, Saint-Petersburg, Russia

⁴ Research Institute of Mechanics of Lobachevsky NNGU, 603600 Nizhny Novgorod, Russia

⁵ Mechanical Engineering Research Institute of Russian Academy of Sciences, Moscow, Russia
e-mail: sav-georgij@yandex.ru

Received March 3, 2022

Revised March 24, 2022

Accepted March 29, 2022

The results of dynamic testing of alumina samples with different graphene content are presented. The tests were carried out using a split Hopkinson rod according to the „Brazilian test“ method at an impact speed of 10 m/s. The optimal value of the graphene content was obtained. The strength characteristics of the alumina nanocomposite with graphene reach a maximum at this value.

Keywords: ceramic composite, graphene, split Hopkinson rod, Brazilian test.

Introduction

The last decade has seen the field of fundamental and applied science in raised interest to ceramic composites based on alumina [1–3]. The sintered coarse-grain ceramics Al_2O_3 is a modern structural material, which is characterized by high values of the melting temperature, the modulus of elasticity, hardness and compressive strength, as well as chemical thermal stability, heat-resistance and corrosion resistance. However, there are properties, which limit its practical use and include low electric conductivity, weak cracking resistance and wear resistance, high brittleness in comparison with the metallic materials. There are several possible solutions of the problem of improving the above-said properties of the ceramics Al_2O_3 . The first one is its structural refinement to a nano-size range, because the less the grain size and more strongly developed the grain structure, then the stronger and the harder the ceramics. The second one means adding either carbon nanoparticles of a various type including graphene [4,5], or ceramics with higher strength characteristics (SiC , TiC , TiN , ZrO_2 , etc.) to it [6].

The graphene composites have a number of unique electrophysical, mechanical, thermal properties [7–10]. The particular interest is paid to a nanocomposite based on nanosized corundum powder and small additives of multi-layer graphene, which is produced by the spark plasma sintering methods (SPS) [9]. The SPS method allows producing the ceramic composite with the density close to a theoretical value and a grain size close to a particle size of the original powder.

At the same time, it is assumed that adding the graphene scales that can be arranged on the grain boundaries of the ceramic matrix can cause significant reduction of brittleness

of the Al_2O_3 composite due to increase in the adhesive properties of submicron elements [9]. Some studies confirm it in the bending static-compression tests [10].

In regard to application of the structural ceramics predominantly in the impact load conditions, for example, in bulletproof vests, fuel pellets [11,12] or in surface coatings of the product elements under the impact loads, an important problem is to determine its strength properties (including cracking resistance) in the conditions of static or dynamic tension or compression. This problem is correlated, first of all, to the shape and sizes of the test specimen, which is often a relatively thin disc of the thickness of 1–8 mm and the diameter of 15–30 mm. With such small sizes it is not possible to perform the standard mechanical tests (excluding determination of microhardness, which will also be presented in the present study). That is why the tests under the static conditions often use an indirect method of determining the index of material tension resistance (the so-called „Brazilian test“ — compression of the disc in a diametrical plane, when the specimen center forms the tensile stresses) [13–16]. This method of the static tests was proposed in 1947 by the Brazilian engineer F. Carneiro and later modified for dynamic loading at the Split Hopkinson Rod (SHR) [16].

The study [3] estimated the dynamic strength of the ceramics by a damage degree of the aluminum plate (the maximum depth of a cavity), on which the alumina specimen rested. The specimen was impacted by the quenched steel striker (the diameter of 6 mm, the height of 22 mm, the apex angle of 30°), having the velocity of 750 ± 15 m/s.

Besides, some indirect dynamic characteristics of the alumina ceramics can be obtained when the specimen

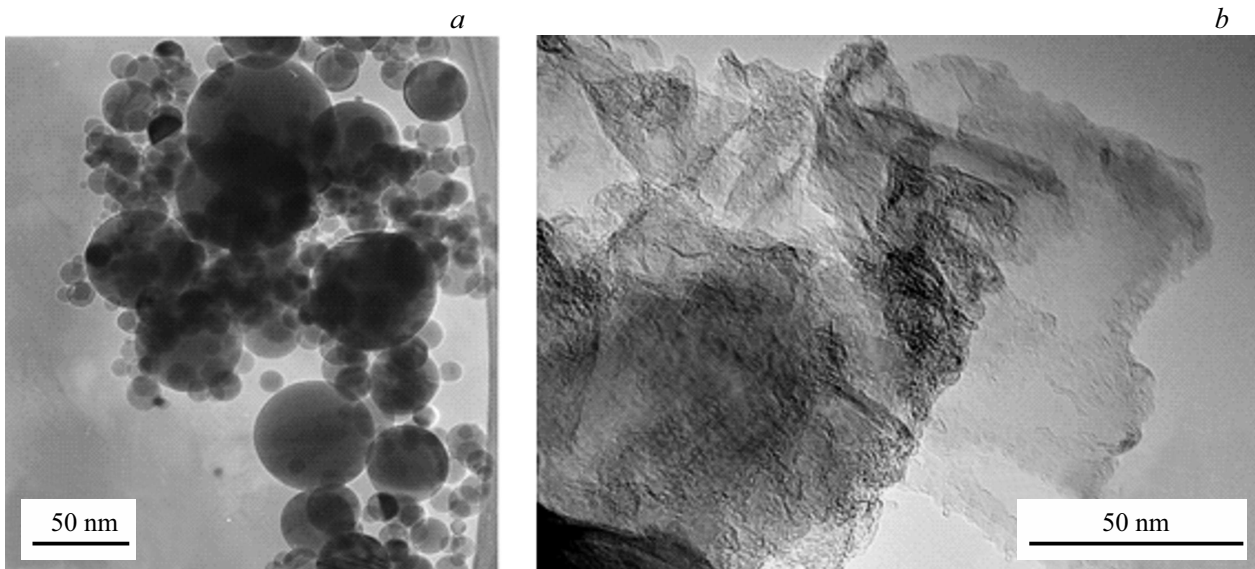


Figure 1. SEM-image of the aluminum powder (a) and the graphene scales (b).

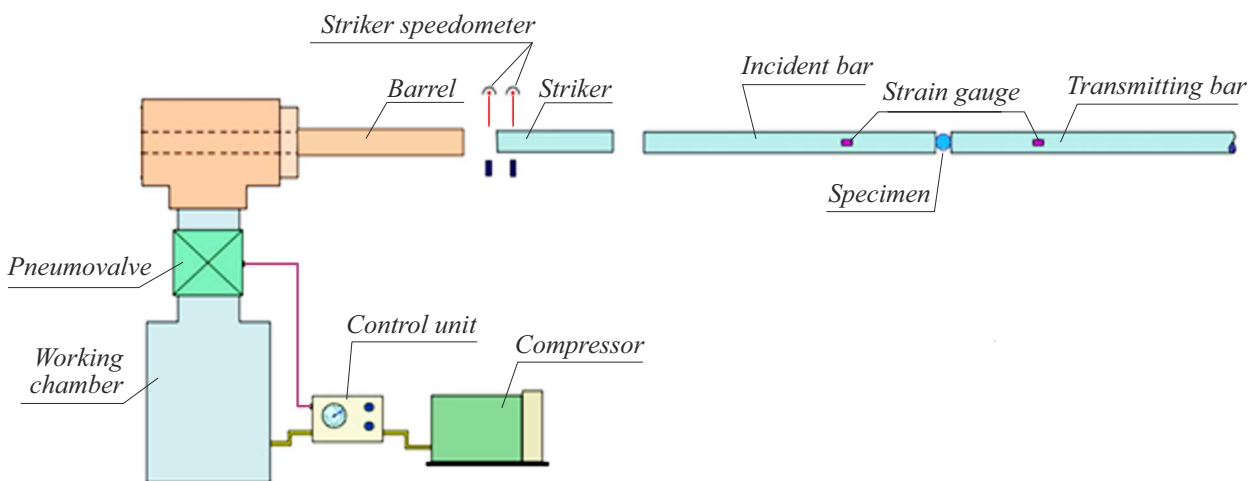


Figure 2. Experimental unit scheme.

is exposed to the electrophysical pulse (the high-voltage discharge and the high-current electron beam) [17].

The purpose of this study is to investigate the influence of the graphene content on the strength and the nature of the fracture $\text{Al}_2\text{O}_3/\text{Graphene}$ (hereinafter — $\text{Al}_2\text{O}_3/\text{G}$) in the impact load conditions nanocomposite.

1. Material and research techniques

The $\text{Al}_2\text{O}_3/\text{G}$ nanocomposite under investigation has been obtained by the method of spark plasma sintering (SPS) of the mixture of the nanosized corundum powder (the particle size of 45 nm) and the small additives of five-layer graphene. The graphene content varied from 0 to 2 wt.%. The test specimens were made as discs of the

diameter of 15 mm and the thickness of 2.3 mm. The initial microstructure of the specimens is shown on Fig. 1.

Before the dynamic tests, the structural morphology of fractures of the sintered specimens was studied using the Hitachi SU8000 field emission Scanning Electron Microscope (SEM). As the studied composite is a dielectric material, the magnetron sputtering method was used to coat the metal with a thin film (10 nm) of the gold/palladium alloy (60/40) [18]. The specimen morphology was investigated taking into account possible influence of the metallic coating on the specimen surface [19]. In the center and at the periphery, the microhardness of the specimens, which are preliminarily grounded and polished to the surface roughness $R_z \leq 1 \mu\text{m}$ was determined using the Isoscan OD device at the load of 2N as being kept under the load for 10 s. The number of the measurements is at least ten for each point.

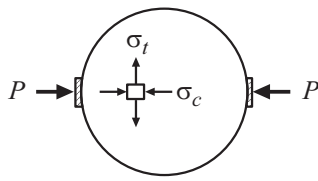


Figure 3. Specimen loading in the „Brazilian test“ diagram.

In order to determine the loading diagrams and the limit fracture characteristics of $\text{Al}_2\text{O}_3/\text{G}$ (the maximum tensile stress) during the dynamic loading, the RSG-20 unit (Fig. 2) with the split Hopkinson Rod was used [20]. The unit is designed to perform „the Brazilian test“ (the compression of the disc in the diametrical plane between the two measurement rods (Fig. 3)) [16].

The cycle of the investigations was performed by using a loading and bearing bars made of high-strength steel with the yield stress of $\sigma_s \sim 2000$ MPa.

In the common tests for compression of the cylindrical specimens the load is applied along the longitudinal axis of the specimen. The splitting experiments for determination of the tensile strength were performed by turning the cylindrical specimen by 90° around the longitudinal axis and the load is applied along the diametrical plane (Fig. 3).

The length of the loading and bearing bars is 1.5 and 3.0 m, respectively. The pulse of elastic deformations, which passes through the specimen to the bearing bar $\varepsilon^T(t)$, allows determining the compressive σ_c and tensile σ_t stresses. The compressive and tensile stresses obtained from solving the Hertz contact problem in the elastic formulation are expressed as follows:

$$\sigma_t = \frac{2P}{\pi HD},$$

$$\sigma_c = \frac{2P}{\pi HD} \cdot \frac{D^2}{r(D-r)},$$

where H — the disc thickness, D — its diameter, r — the current coordinate along the specimen radius. The contact force P is determined by the dependence

$$P = E_b S_b \varepsilon^T(t),$$

where E_b — the Young modulus of the rod material, S_b — the section area of the measurement rod.

The velocity of impact on the loading rod was 10 ± 0.1 m/s. The tests were made at 20°C . The fracture process in time was fixed by means of the video camera at the rate of 50,000 frames per second. The two specimens of each graphene content were tested.

2. Results and discussion thereof

2.1. Microhardness

The results of microhardness measurement as curves in the center and at the periphery of the specimen are

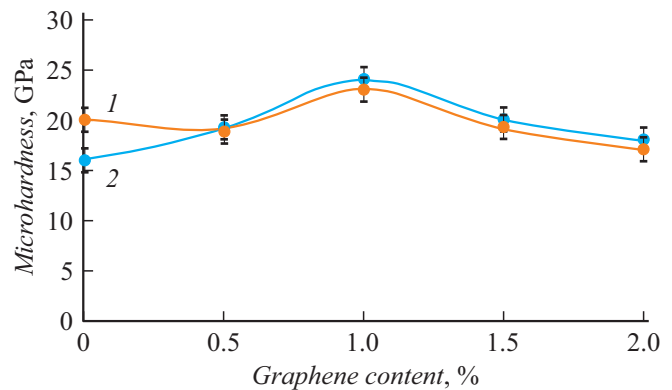


Figure 4. Dependence of the microhardness on the graphene content: 1 — the center, 2 — the periphery.

shown on Fig. 4 depending on the graphene content. It is clear that the microhardness behavior is dome-shaped with the microhardness maximum of about 23.9 GPa at the graphene content of 1 wt.%. Despite locality of the method of microhardness measurement and its possible error, the curves 1 and 2 are almost the same. Generally, these results are indicative of the diametrical homogeneity of the structure of the graphene-sintered specimens. The exception is the non-graphene specimen, wherein the microhardness in the periphery area is noticeably higher than in the center. Most likely, it indicates the heterogeneity of the distribution of the temperature and the compressive axial stresses in sintering, which are leveled by graphene input. The range of found values of the microhardness 16–24 GPa is quite close to the one specified in the study [21], wherein, however, there is no maximum on the curve of the dependence of the microhardness on the graphene content. Probably, this difference is correlated to the fact that a reinforcing additive was graphene oxide GO, which is less agglomerated.

2.2. Fractography

Figure 5 shows the SEM images of the fracture surface in the specimen with the various graphene content. It is clear that the addition of graphene in the sintered specimens results in disappearance of porosity (Fig. 5, a and b) and appearance of micron-size agglomerates (Fig. 5, c).

In doing so, the average grain size is increased almost by two orders in comparison with the particle size in the initial powder. The grain growth is correlated to sintering heating and particularly noticeable for the graphene specimens, which can be explained by its higher thermal conductivity than for the pure ceramics.

2.3. Results of specimen HCR tests

The time dependences of the tensile stresses in the specimen loading plane are exemplified on Fig. 6. The kind of the „stress–time“ diagrams is indicative of an almost linear dependence of the stress on time within the

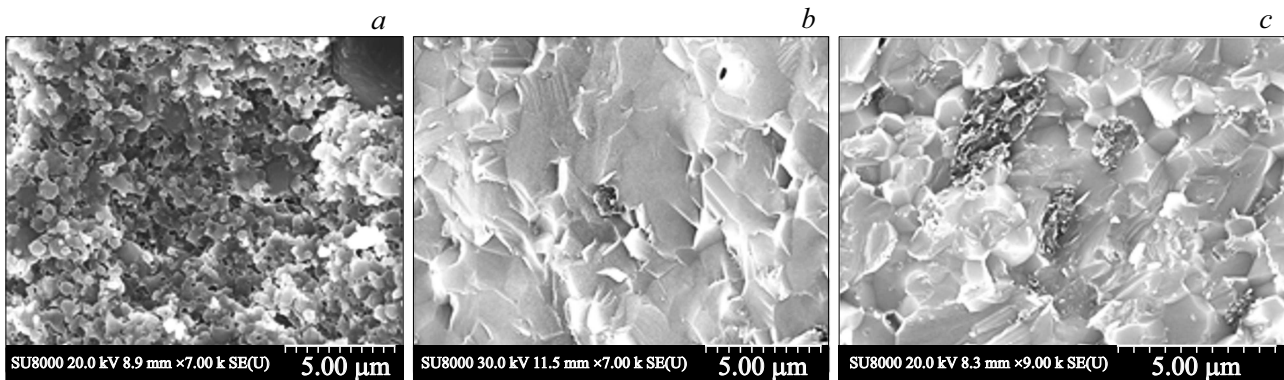


Figure 5. SEM-images of the specimen fracture surface with the graphene content, wt.%: *a* — 0, *b* — 0.5, *c* — 1.5.

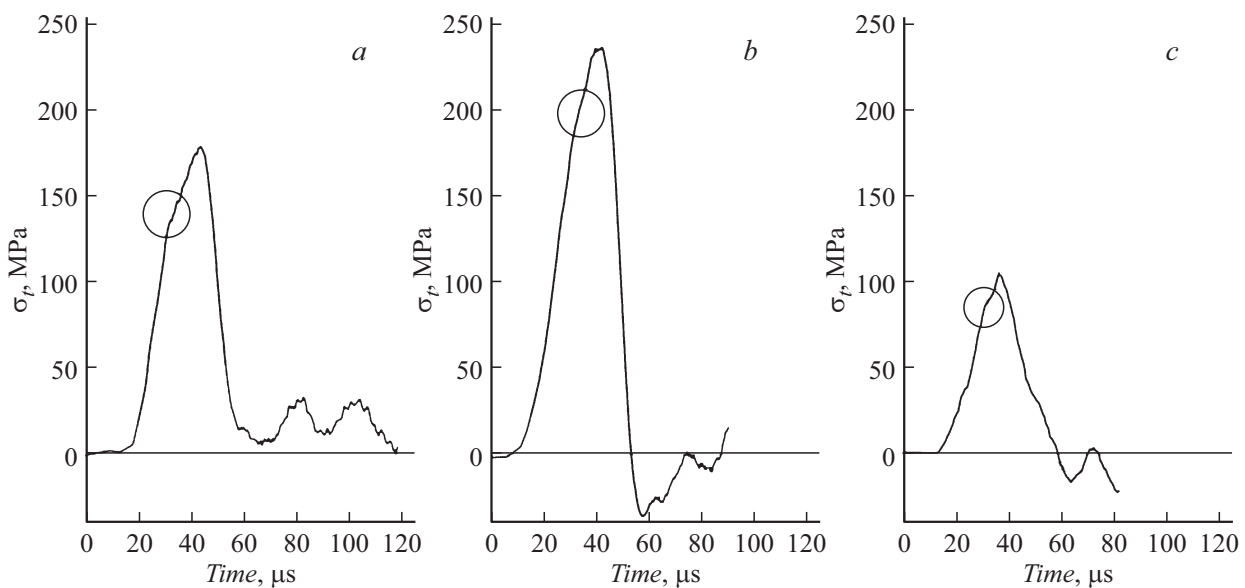


Figure 6. Specimen loading diagrams with the graphene content, wt.%: *a* — 0, *b* — 0.5, *c* — 1.5.

loading area. However, the upper part of the loading curve has insignificant change of the slope angle, which can indicate some manifestation of the plastic properties of the composite.

It is clear from Fig. 6 that after the specimen rupture the curve $\sigma(t)$ decreases to zero to be followed by evident oscillations of this curve near the zero line. These oscillations are caused by generation of a steep rear front at the compression pulse passed into the bearing measurement rod with the specimen fracture. It results in high-frequency harmonics in the signal spectrum. As the signal is recorded by strain sensors at some distance from the specimen, the pulse as progressing is somewhat distorted when moving along the measurement rod due to dispersion effects. The high-frequency harmonics lag behind the main package. It is them that we see at a pulse tail as oscillations of the zero line. These oscillations are not related to the material properties and result from features of the measurement system used [22].

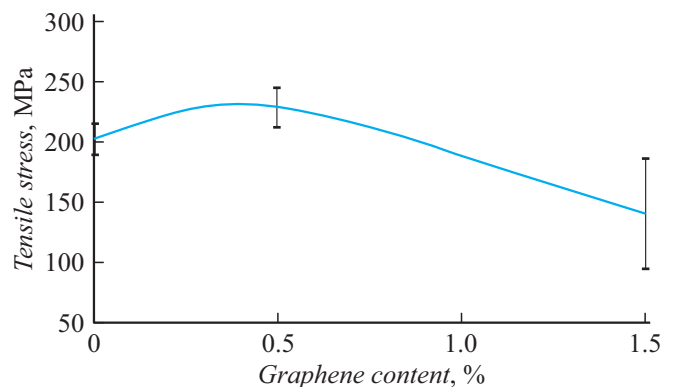


Figure 7. Dependence of the maximum tensile stress on the graphene content.

It should be noted that [16] shows the test results for the „Brazilian test“ method for alumina of 96% purity. However, in contrast to the present study, the authors of

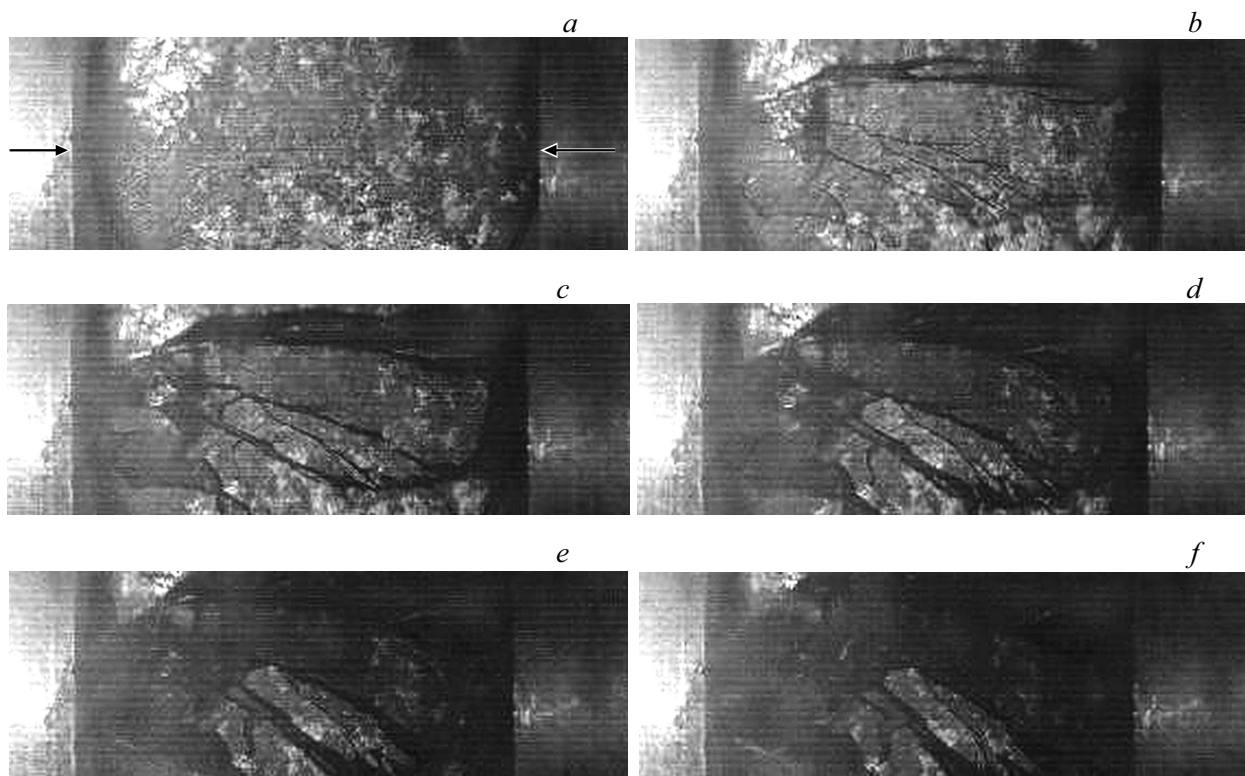


Figure 8. Process of fracture of the specimen $\text{Al}_2\text{O}_3/1.5 \text{ wt.}\% \text{ G}$ (the arrows show the compression direction). Explanations are given in the text.

Results of specimen tests

№ specimen	Content of graphene, wt.%	Velocity of impact, m/s	Maximum tensile stress σ_t , MPa
1	0	9.9	191
2		10.1	216
3	0.5	9.9	213
4		10.0	246
5	1.5	10.0	187
6		10.2	95

the study [16] have observed only the linear elastic behavior of the material, which can be explained by no graphene and different purity of the alumina.

The dependence of the maximum tensile stresses on the graphene content is shown on Fig. 7 and in the Table. The results of the studies of the Figs. 4 and 7 are compared to show that there is still a trend of change of the mechanical properties (the microhardness and the maximum tensile stress): with increase in the graphene content the values of the property characteristics increase to the maximum and then reduce. This reinforcing graphene influence (up to 40%) in the Al_2O_3 -based nanocomposites

was also observed for other mechanical characteristics, like bending strength [23], fracture toughness and elastic modulus [24]. However, the maximum of the fracture stress and microhardness is attained at the various graphene content — 0.5 and 1.0 wt.%, respectively. The difference can be correlated to the locality of the acting load when measuring the microhardness, as well as to the fact that in the microhardness measurements the portion of the tensile stresses is low in comparison with the tangent stresses created in the deformed material [25], while, vice versa, in the tests as per „the Brazilian test“ the portion of the shear stresses is small in comparison with the tensile stresses. The close values of the maximum tensile stress $\sigma_t = 190 \pm 40 \text{ MPa}$ for the pure ceramics have been obtained by the authors of the study [16], thereby definitely matching the values obtained in the present study.

It is also clear from Fig. 7 that with increase in the graphene content the dispersion of the maximum tensile stress values is also increased, which can be correlated to graphene agglomerates appearing to cause the structural heterogeneity of the composites obtained. Of course, we can assume this cause with some portion of the probability correlated to the small statistics of the tests.

Figure 8 shows (left to right, top to bottom) frames of the process of fracture of the specimen (as there are a big number of the frames, the Fig. 8 shows the selected frames), which is shot by the fast video camera. The video of the specimen fracture process (Fig. 8) was recorded at its flat

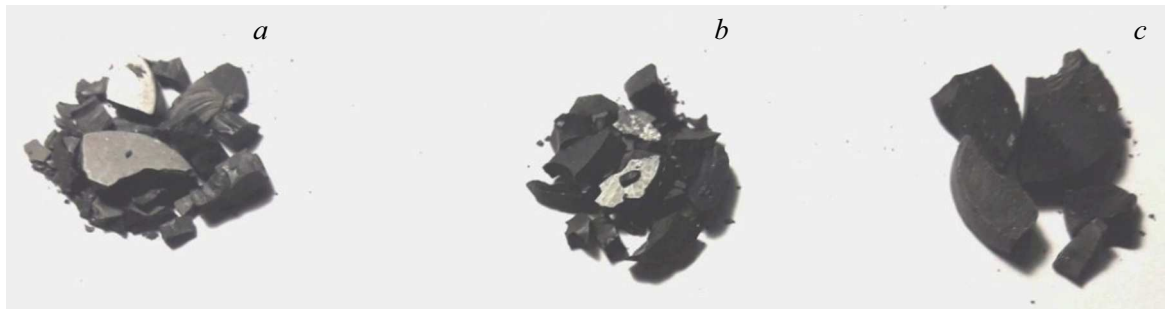


Figure 9. Fragments of the specimens after the tests.

part (as shown on the diagram of Fig. 3). The specifics of the high-speed video recording is that the increase in the time resolution of the camera (increase in a frame frequency) necessitates the decrease in the space resolution (an image size). Searching a compromise between these parameters to obtain a sufficient number of the frames representing the time behavior of the process in interest, requires to focus only on the part of the specimen, in which this process is localized. In our case, we have observed behind the diametrical splitting line of the specimen, which connects contact points with the measurement rods. Due to equipment limitations of the camera, the specimen was not entirely inside the frame.

It should be noted that despite the duration of the pulse passed through the specimen is about $40 \mu\text{s}$, the specimen is loaded substantially longer. The split rod system is loaded by the compression pulse, which duration is determined by the double wave run inside the striker and can be evaluated as follows: $T = 2L/c$, here L — the striker length, c — the rod speed of sound inside the striker material. The experiments have used the steel striker of the 300 mm length. Thus, the duration of one loading was $T = 2 \cdot 0.3/4850 \approx 124 \mu\text{s}$. Figure 8 shows the picture of fracture of the composite with 1.5% G for the entire loading process. When judging by the time dependence of the force, then Fig. 8, c illustrates the state when the specimen is already fractured with no resistance to deformation.

As follows from the video recording frames, the intense fracture process starts with the periphery area of the disc (Fig. 8, b) and only after that it embraces its central part (Fig. 8, c–f).

This process behavior was typical for all the specimens regardless of the graphene content. It can be assumed that the beginning of the process development from the periphery area is correlated to the effects of contact friction, which affects the stress-strain state in the contact area of the measurement rods and the specimen.

All the specimens excluding one were fractured into a multitude of small and fine fragments (Fig. 9, a, the specimen № 2 and b — the specimen № 4), while the specimen № 6 (Fig. 9, c) has fractured into several large and, probably, fine fragments, as follows from Fig. 8.

Recently, the resistance of this composite to the electro-physical pulses under impact of the high-current electron beam and the high-voltage discharge was investigated to show that increase in the graphene content within the range 0.5–2.0 wt.% contributes to increase in the number of the fragments in fracture [18]. The said study has obtained the following dependence between the number of the fragments, the critical tensile stress ($\sigma_{cr} = \sigma_r$) and the material crack resistance K_{IC} :

$$N_e \approx \frac{d^2}{4\beta} \cdot \frac{1}{3} \left(\frac{\sigma_{cr}}{K_{IC}} \right)^4,$$

where β — the match coefficient from the relationship for the area equation (πd^2) = $N_e \beta a_e^2$, here d — the specimen diameter, a_e — the typical size of the fragment. Thus, the result obtained in the present study fully complies with the specified relationship: the less critical stress, the less the number of the fragments.

Conclusion

Based on the performed studies of the influence of the graphene additives on the microhardness and their dynamic strength and the fracture of the alumina under the high-speed loading, the following conclusions can be made:

1. The obtained experimental curves of the dependences of the microhardness and the maximum tensile stress on the graphene content have maximum and in some degree are quasi-similar curves.

2. The optimum graphene content, at which the strength characteristics of the nanocomposite are at their maximum is 0.5 and 1.0 wt.%, respectively, for the tensile stress and the microhardness. 3. The increase in the graphene content results in the increase in the dispersion in the maximum tensile stress values, which can be correlated with well-defined graphene agglomeration.

Conflict of interest

The authors declare that they have no conflict of interest.

References

- [1] D. de Faoite, D.J. Browne, F.R. Chang-Díaz, K.T. Santon. *J. Mater. Sci.*, **47** (10) (2012).
- [2] A.V. Nomoev. *Pis'ma v ZhTF*, **36** (21), 46 (2010) (in Russian).
- [3] A.M. Bragov, V.N. Chuvil'deev, V.N. Melekhin, M.S. Boldin, V.V. Balandin, A.V. Nokhrin, A.A. Popov. *PMTF*, **61** (3), 207 (2020) (in Russian).
- [4] A. Centeno, V.G. Rocha, B. Alonso, A. Fernández, C.F. Gutierrez-Gonzalez, R. Torrecillas, A. Zurutuza. *J. Eur. Ceram. Soc.*, **33**, 3201(2013).
- [5] B. Lee, M.Y. Koo, S.H. Jin, K.T. Kim, S.H. Hong. *Carbon*, **78**, 212 (2014).
- [6] M.S. Boldin, N.V. Sakharov, S.V. Shotin, V.N. Chuvil'deev, A.V. Nokhrin, D.N. Kotkov, A.V. Pisklov. *Vestnik Nizhegorodskogo un-ta im. N.I. Lobachevskogo*, **6** (1), 32 (2012) (in Russian).
- [7] V.R. Akhil Raj, K. Hadagalli, P. Jana. *J. Mater. Eng. Perform*, **30**, 1234 (2021).
- [8] H.J. Kim, S.-M. Lee, Y.-S. Oh, Y.-H. Yang, Y.S. Lim, D.H. Yoon, Ch. Lee, J.Y. Kim, R.S. Ruoff. *Sci. Rep.*, **4**, 5176 (2014).
- [9] A. Borrell, R. Torrecillas, V.G. Rocha, A. Fernández. *Wear*, **274**, 94 (2012).
- [10] S. Stankovich, D.A. Dikin, G.H. Dommett, K.M. Kohlhaas, E.J. Zimney, E.A. Stach, R.D. Piner, S.T. Nguyen, R.S. Ruoff. *Nature*, **442**, 282 (2006).
- [11] Y.B. Adebayo, G.I. Douglas. *J. Mater. Sci.*, **36** (20), 4995 (2001).
- [12] R. Azarafza, A. Arab, A. Mehidpoor. *Intern. J. Adv. Design and Manufactur. Technol.*, **5** (5), 83 (2012).
- [13] V.Yu. Goltsev, A.V. Osintsev, A.S. Plotnikov. *Lett. Mater.*, **7** (1), 21 (2017).
- [14] Q.Z. Wang, X.M. Jia, S.Q. Kou, Z.X. Zhang, P.A. Lindqvist. *J. Rock Mechanics and Mining Sciences*, **41** (2), 245 (2004).
- [15] ASTM D3967-95a. Standard Test Method for Splitting Tensile Strength of Intact Rock Core Specimens.
- [16] T. Rodriguez, C. Navarro, V. Sanchez-Galvez. *J. Physique*, **IV**, 101 (1994).
- [17] A.V. Kuznetsov, V.A. Morozov, G.G. Savenkov, V.V. Stolyarov. *ZhTF*, **91** (3), 484 (2021) (in Russian).
DOI: 10.21883/TP.2022.06.54417.47-22
[A.V. Kuznetsov, V.A. Morozov, G.G. Savenkov, V.V. Stolyarov. *Tech. Phys.*, **66** (3), 470 (2021).
DOI: 10.1134/S1063784221030154]
- [18] D. de Faoite, D.J. Browne, F.R. Chang-Díaz, K.T. Santon. *J. Mater. Sci.*, **47** (10), 4211 (2012).
- [19] A.S. Kashin, V.P. Ananikov. *Russ. Chem. Bull.*, **60**, 2602 (2011).
- [20] A.M. Bragov, A.K. Lomunov. *Ispol'zovanie metoda Kol'skogo dlya issledovaniya protsessov vysokoskorostnogo deformirovaniya materialov razlichnoi fizicheskoi prirody*. (Izd-vo Nizhegorodskogo un-ta, Nizhny Novgorod, 2017) (in Russian).
- [21] B. Lee, M.Y. Koo, S.H. Jin, K.T. Kim, S.H. Hong. *Carbon*, **78**, 212 (2014).
- [22] A.M. Bragov, A.K. Lomunov, D.A. Lamzin, A.Yu. Konstantinov. *Continuum Mech. Thermodyn.*, (2019).
DOI: 10.1007/s00161-019-00776-0
- [23] E.A. Klyatskina, A. Borrell, E.G. Grigoriev, A.G. Zholnin, M.D. Salvador, V.V. Stolyarov. *J. Ceram. Soc. Tech.*, **9** (3), 215 (2018).
- [24] H. Porwal, P. Tatarko, S. Grasso, J. Khaliq, I. Dlouhý, M.J. Reece. *Carbon*, **64**, 359 (2013).
- [25] Ya.B. Fridman. *Mekhanicheskie svoistva metallov. Ch. 2. Mekhanicheskie ispytaniya. Konstruktsionnaya prochnost'* (Mashinostroenie, M., 1974) (in Russian).